Journal of Hazardous Materials 286 (2015) 509–516

Contents lists available at ScienceDirect

Journal of Hazardous Materials

journal homepage: www.elsevier.com/locate/jhazmat

Fabrication and characterization of PbO_2 electrode modified with $[Fe(CN)_6]^{3-}$ and its application on electrochemical degradation of alkali lignin

Xu Hao[a], Yuan Quansheng[a], Shao Dan[a], Yang Honghui[a,b], Liang Jidong[a], Feng Jiangtao[a,*], Yan Wei[a,b,**]

[a] Department of Environmental Science and Engineering, Xi'an Jiaotong University, Xi'an 710049, China
[b] The State Key Laboratory of Multiphase Flow in Power Engineering, Xi'an Jiaotong University, Xi'an 710049, China

HIGHLIGHTS

- $[Fe(CN)_6]^{3-}$ is used to modify PbO_2 electrode by the electro-deposition method.
- $[Fe(CN)_6]^{3-}$ addition can enhance the stability of lead dioxide electrodes.
- $[Fe(CN)_6]^{3-}$ addition can enhance the electrochemical activity of lead dioxide electrodes.
- $[Fe(CN)_6]^{3-}$–10 mM electrode shows the highest electrochemical activity.

ARTICLE INFO

Article history:
Received 9 October 2014
Received in revised form
18 December 2014
Accepted 31 December 2014
Available online 5 January 2015

Keywords:
PbO_2 electrode
$[Fe(CN)_6]^{3-}$
Electrochemical characterization
Alkali lignin
Electrochemical degradation

ABSTRACT

PbO_2 electrode modified by $[Fe(CN)_6]^{3-}$ (marked as FeCN–PbO_2) was prepared by electro-deposition method and used for the electrochemical degradation of alkali lignin (AL). The surface morphology and the structure of the electrodes were characterized by scanning electronic microscopy (SEM) and X-ray diffraction (XRD), respectively. The stability and electrochemical activity of FeCN–PbO_2 electrode were characterized by accelerated life test, linear sweep voltammetry, electrochemical impedance spectrum (EIS) and AL degradation. The results showed that $[Fe(CN)_6]^{3-}$ increased the average grain size of PbO_2 and formed a compact surface coating. The service lifetime of FeCN–PbO_2 electrode was 287.25 h, which was longer than that of the unmodified PbO_2 electrode (100.5 h). The FeCN–PbO_2 electrode showed higher active surface area and higher oxygen evolution potential than that of the unmodified PbO_2 electrode. In electrochemical degradation tests, the apparent kinetics coefficient of FeCN–PbO_2 electrode was 0.00609 min^{-1}, which was higher than that of unmodified PbO_2 electrode (0.00419 min^{-1}). The effects of experimental parameters, such as applied current density, initial AL concentration, initial pH value and solution temperature, on electrochemical degradation of AL by FeCN–PbO_2 electrode were evaluated.

1. Introduction

Electrochemical degradation method has been developed for decades and reached a promising stage in degrading toxic or bio-refractory organic pollutants efficiently because of its simplicity, easy control, strong oxidation performance and environmental compatibility [1–4]. Electrode material is crucial for the electrochemical degradation process [5]. The degradation efficiency and mineralization degree are strongly dependent on the properties of the selected electrode. Thus, a lot of efforts have been paid to exploring the novel electrode materials, especially "non-active" anodes, which show high potential on oxygen evolution and high activity on producing hydroxyl radicals (•OH) [6].

Currently, the most typical "non-active" electrodes are dimensionally stable anodes (DSA) that is widely used due to its easy preparation and high cost-efficiency. Among these reported DSA electrodes, PbO_2 electrode is considered as an excellent metal oxide electrode for its high chemical stability in corrosive media, relatively high over-potential in oxygen evolution reaction and low price compared with noble metal electrodes [7]. Therefore, PbO_2 anode material has attracted more and more attention in the field of electrochemical degradation treatment. For instance, PbO_2 anode has been employed to oxidize recalcitrant organic pollutants such as metalaxyl [8], methyl red [9], lignin [10,11], triazole fungicides [12] sulfamethoxazole [13] and *p*-nitrophenol [14] by •OH produced during water electrolysis.

Much effort has been paid on the modification of PbO_2 electrode for further improvement of its performance in the electrochemical degradation of organic pollutants in water. A frequently-used method is to modify the PbO_2 layer with some

* Corresponding author. Fax: +86 29 82664731.
** Corresponding author at: Department of Environmental Science and Engineering, Xi'an Jiaotong University, Xi'an 710049, China. Fax: +86 29 82664731.
E-mail addresses: fjtes@mail.xjtu.edu.cn (X. Hao), yanwei@mail.xjtu.edu.cn (Y. Wei).

http://dx.doi.org/10.1016/j.jhazmat.2014.12.065
0304-3894/

elements [4,7], such as Bi [15,16], Fe [14,17], Ce [13,18–21], Zr [22–26], Cu [5], Pr [27], La [20,28], and F [25,29–33]. The results showed that these modifications could obviously accelerate the electrochemical oxidation process and enhance the electrode stability in corrosive solutions. To the best of our knowledge, F^- was the only anion studied in the reports for PbO_2 electrode modification. $[Fe(CN)_6]^{3-}$ anion is an excellent electrochemical redox ion. In the electrochemical cell, it will migrate to the anodic area due to the electrostatic attraction. If $[Fe(CN)_6]^{3-}$ anion is added into the PbO_2 electro-deposition solution, it may dope into the PbO_2 matrix due to the migration, which would fabricate a novel doped PbO_2 electrode. The as-prepared electrode may show different performance compared with the native PbO_2 electrode.

Lignin is a tridimensional polymer consisting of 9-carbon phenol propane units, non-uniformly linked together by different types of bonds (alkyl–aryl, alkyl–alkyl and aryl–aryl ether bonds) [34]. It accounts for approximately 20–30% of wood, and is the major by-product in pulp and paper industrial wastewater [10]. Lignin and its derivatives are the principal contaminants in the effluent of the pulp and paper industry, causing high COD value and colorful effluent [11]. Besides, water is unrecyclable in pulp and paper mills because the accumulation of lignin and its derivatives in the recycled water could cause decline in paper quality [10]. Thus, there is a great interest in lignin degradation to meet effluent discharge standards and water recycles requirements. However, the degradation of lignin and its derivatives in industrial effluent is relatively complex due to its relatively high resistance toward conventional chemical and biochemical degradation methods [35]. Therefore, an effective lignin removal approach with low cost and no secondary pollution is significant.

As mentioned above, electrochemical degradation method has been described as an effective alternative in wastewater treatment for its numerous advantages. Our group [10,36] and other scientists [11,34,37] confirmed the feasibility of degrading lignin by electrochemical degradation process. However, there is no report using the $[Fe(CN)_6]^{3-}$ modified PbO_2 electrode as the anode to treat lignin. Therefore, in the present work, for the sake of studying the effect of $[Fe(CN)_6]^{3-}$ modification, titanium-based β-PbO_2 electrodes were fabricated by electrochemical deposition. The morphology, crystalline structure, stability, and electrochemical performance of the as-prepared electrode were characterized. In order to evaluate its electrocatalytic activity, alkali lignin (AL) was employed as a toxic biorefractory model organic pollutant for electrochemical degradation. Finally, the effects of applied current density, initial AL concentration, and initial pH value on the decay kinetics were systematically studied.

2. Materials and experiments

2.1. Materials

All chemicals used in the experiments were analytical reagent grade or higher and used without further purification. Titanium (Ti) plate (purity: 99.6%, BaoTi Co., Ltd., China) with 0.5 mm-thickness was used in this study. Deionized water prepared from an EPET-40TF system (EPET Co., Ltd., Nanjing, China) was used for aqueous solution preparation and Ti plate washing.

2.2. Electrode preparation

Ti plates with a dimension of 2 cm × 4.5 cm × 0.5 mm were used as the electrode substrate. Prior to the electrode preparation process, Ti plates were mechanically polished with 1000-grid abrasive papers, and then rinsed with deionized water. The plates were subsequently pretreated ultrasonically in the solution composed of acetone and 1 mol L^{-1} NaOH (1:1 v/v) for 30 min to remove organic residues from the surface. Then the plates were etched in 10 wt% oxalic acid at 98 °C for 120 min. The plates were then rinsed thoroughly with deionized water and dried for use.

The inner Sb–SnO_2 layer was prepared by dip-coating plus thermal deposition method. The precursor solution for the inter metal oxide layer was prepared by dissolving 10 wt% $SnCl_4{\cdot}6H_2O$ and 1 wt% $SbCl_3$ in a solution consisting of 10 mL *n*-butanol, 10 mL *iso*-propanol, 10 mL ethanol and 2 mL hydrochloric acid (37%). The precursor solution was brushed onto the titanium plates, and then calcined in a muffle oven (KLS-1100X, Hefei Kejing Co., Ltd., China) at 450 °C for 15 min. This procedure was repeated 10 times. The electrode was then annealed at 450 °C for 1 h. The average oxide loading amount of the dip coating method was 1.1 mg cm^{-2}.

The electro-deposition of α-PbO_2 layer was carried out to prepare an interlayer between the inner Sb–SnO_2 layer and the surface β-PbO_2 layer. The deposition solution was composed of 0.11 mol L^{-1} PbO and 3.5 mol L^{-1} NaOH. The prepared Ti/Sb–SnO_2 electrode was used as the anode, and the copper plate with the same surface area was used as the counter cathode. The deposition process was carried out in an undivided cylindrical vessel with a current density of 10 mA cm^{-1} for 30 min. The solution was maintained at 40 °C with water bath and stirred by a magnetic stirring bar in the deposition process. The electrochemical deposition system was powered by a DC power source. After the deposition process, the as-prepared Ti/Sb–SnO_2/α-PbO_2 electrodes were rinsed thoroughly with deionized water. The average amount of α-PbO_2 oxide on the electrode surface was 23 mg cm^{-2}.

The surface β-PbO_2 layer was coated on the Ti/Sb–SnO_2/α-PbO_2 electrode via electrochemical deposition process. The deposition solution was composed of 0.5 mol L^{-1} $Pb(NO_3)_2$ and proper amount of dopant. The solution pH was adjusted to 2.0 with concentrated HNO_3. The deposition processes were carried out at 65 °C for 120 min, and the current density was controlled at 10 mA cm^{-1}. The copper plate with the same size was used as the counter cathode. $K_3[Fe(CN)_6]$ was added into the deposition solution as the dopant. The fabricated electrodes were marked as PbO_2 and FeCN–PbO_2 for undoped electrode and $[Fe(CN)_6]^{3-}$-doped electrode, respectively. The dopant concentration was 5.0, 7.5, 10.0, 15.0 and 20.0 mmol L^{-1}, respectively. The average amount of FeCN–PbO_2 oxide on the electrode surface is 88.8 mg cm^{-2} which is higher than that of PbO_2 electrode (58.8 mg cm^{-2}).

2.3. Characterization

The morphology of samples was characterized by scanning electron microscopy (SEM, JEOL, JSM-6390A). X-ray diffraction (XRD, D/MAX-2400X, Rigaku) analysis was performed using a diffractometer with Cu-Kα radiation, with an accelerating voltage of 40 kV and the electron probe current of 40 mA.

All electrochemical measurements were carried out on the electrochemical workstation (CHI 660D, Shanghai Chenhua, China) with a three-electrode cell at room temperature. The PbO_2 and FeCN–PbO_2 electrodes were served as the working electrodes, respectively. Copper sheet was served as the counter electrode and Ag/AgCl electrode was served as the reference electrode. Linear sweep voltammetry was performed to obtain their oxygen evolution potential in 0.5 mol L^{-1} H_2SO_4 solution with a scan rate of 20 mV s^{-1}. Cycle voltammetry curves were recorded in the range of 0–2 V in 0.5 mol L^{-1} H_2SO_4 solution. The voltammetric charge quantities of different electrodes were calculated by the cycle voltammetry results. EIS measurements were carried out at a measurement potential of 1.8 V in 0.5 mol L^{-1} H_2SO_4 solution, the frequencies swept from 10^5 Hz to 0.01 Hz with an applied sine wave of 5 mV amplitude.

Anti-corrosion performance of the electrodes was determined using accelerated lifetime test with a current density of 500 mA cm^{-2} in 3 mol L^{-1} H_2SO_4 solution at room temperature. The temperature of the H_2SO_4 solution was kept at 45 ± 2 °C due to the ohmic heating. During the accelerated lifetime test, the cell voltage was measured automatically by the CHI 660D electrochemical workstation, and the test was considered to be completed when the cell voltage was higher than 10 V.

2.4. Electrochemical oxidation

The bulk electrochemical oxidation tests were conducted in batch using an undivided electrolytic cell under galvanostatic condition supplied by a WYK-303B potentiostat/galvanostat. The prepared electrodes served as the anodes, and the cathode was copper sheet (2 cm × 4.5 cm), with a distance of 2.0 cm between the two electrodes. 0.1 mol L^{-1} Na_2SO_4 was used as the supporting

electrolyte. The experiments were carried out with a magnetic stirrer for 120 min. During the experiments, liquid samples were withdrawn from the electrolytic cell every 20 min for the UV–vis analysis (Agilent 8453). The UV–vis absorption at 280 nm is proportional to the concentration of AL, and the decrease of the absorbance over time is confirmation of the lignin oxidation process. The UV_{280} removal efficiency of AL in electrochemical oxidation can be calculated as follows:

$$UV_{280}\text{removal efficiency}=\frac{A_0 - A_t}{A_0} \times 100\% \quad (1)$$

where A_0 is the absorbance value in 280 nm of initial wastewater sample and A_t is the absorbance value in 280 nm of the wastewater samples at the given time t, respectively.

The chemical oxygen demand (COD) was measured by a commercial COD detector (Multi Direct, Lovibond). The energy consumption (EC_{COD}, kW h $gCOD^{-1}$) was calculated as follows:

$$EC_{COD} = \frac{50}{3} \times \frac{U_{cell} \times I \times t}{V \times \Delta COD} \quad (2)$$

where U_{cell} is the average cell voltage (V), I is the current during the reaction (A), t is the electrolysis time (min), and V is the volume of the treated solution (mL), ΔCOD is the removal COD value during the electrochemical degradation process (mg L^{-1}).

3. Results and discussion

3.1. Electrode characterization

3.1.1. Effect of dopant concentration

In order to find out an appropriate dopant concentration for the PbO_2 modification, different amount of $K_3[Fe(CN)_6]$ were added into the electro-deposition solution. As shown in Fig. 1, when the dopant concentration was 10.0 mmol L^{-1}, the UV_{280} removal efficiency reached the highest value.

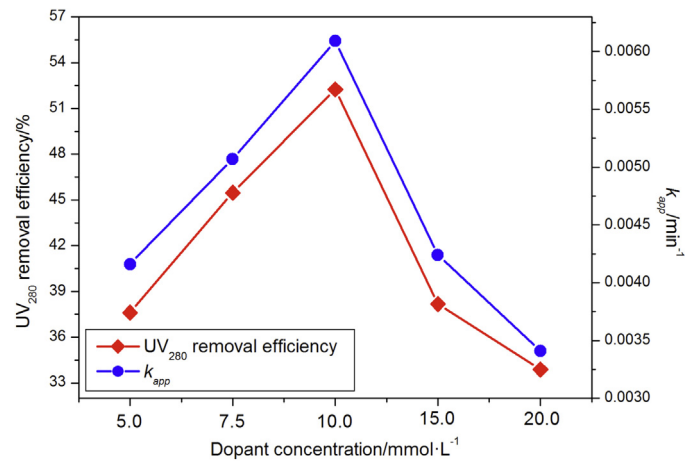

Fig. 1. The effect of the dopant concentration on UV_{280} removal efficiency and kinetics coefficient of AL electrochemical degradation (initial pH: 7; applied current density: 20 mA cm^{-2}; AL concentration: 200 mg L^{-1}; solution temperature: 20 °C).

The curves of the normalized absorbance value at 280 nm with degradation time are shown in the semilogarithmic plots in Fig. S1. According to the good linear correlation between the logarithms values of the normalized absorbance value and treatment time, the oxidation reaction fits pseudo first-order kinetics, and the rate equation for the degradation of alkali lignin can be expressed as follows:

$$A_t = A_0 \times e^{-k_{app}t} \quad (3)$$

where k_{app} is the apparent kinetics coefficient. One can see in Fig. 1 that the highest k_{app} value was achieved under the dopant concentration of 10.0 mmol L^{-1}. These results indicated that the appropriate dopant concentration for the PbO_2 modification was

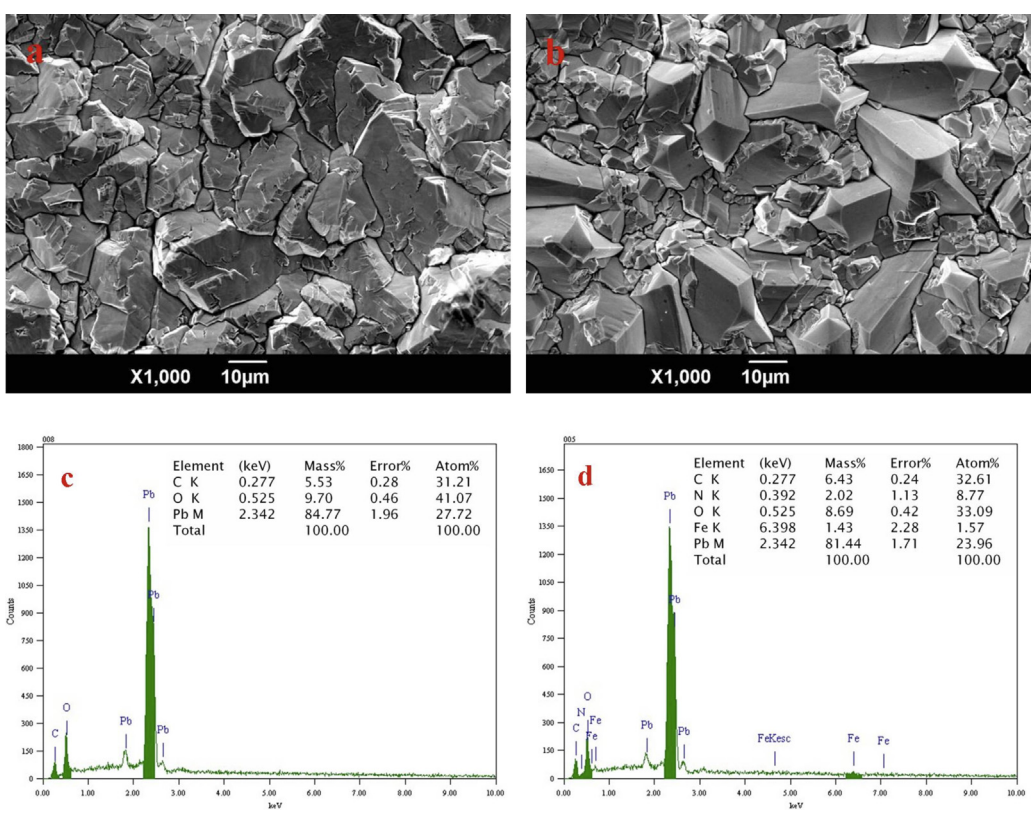

Fig. 2. SEM photographs and EDS result of PbO_2 electrodes (a, c), FeCN–PbO_2 (b, d).

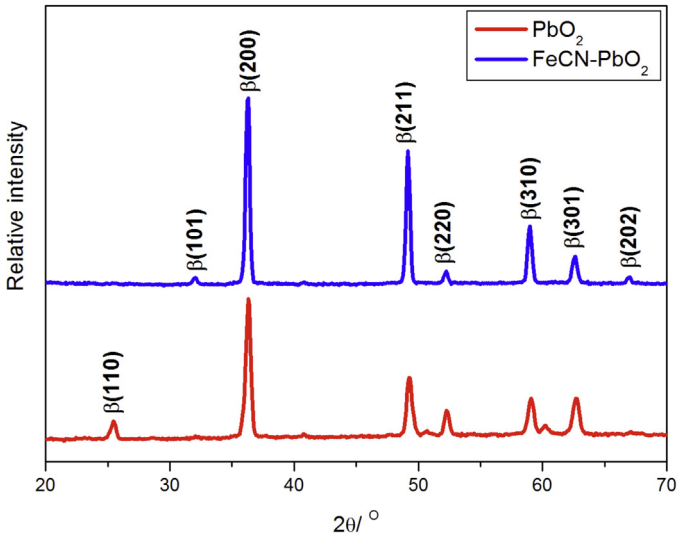

Fig. 3. XRD patterns of PbO_2 and FeCN–PbO_2 electrodes.

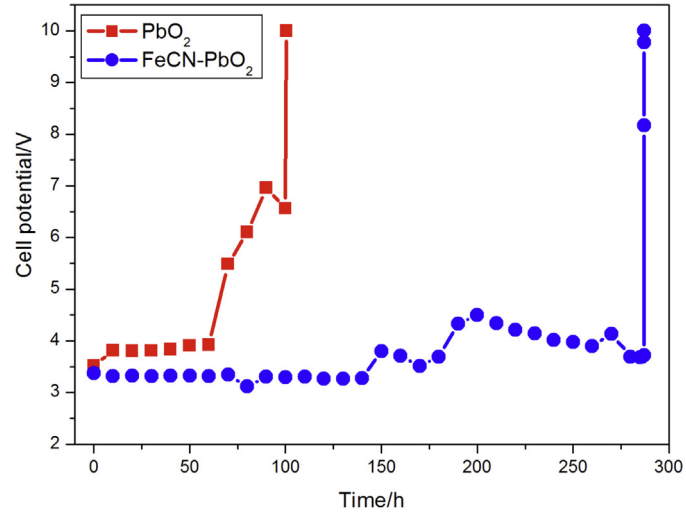

Fig. 4. Accelerated life test of PbO_2 electrode and FeCN–PbO_2 electrode in 3 mol L^{-1} H_2SO_4 solution at current density of 500 mA cm^{-2}.

10.0 mmol L^{-1}. The following FeCN–PbO_2 electrode was fabricated with the dopant concentration of 10.0 mmol L^{-1}.

3.1.2. Surface morphology of PbO_2 electrodes

Fig. 2 shows the SEM micrographs and EDS results of PbO_2 and FeCN–PbO_2. Fig. 2a displays the morphology of the surface layer of the PbO_2 electrode which is coarse, uneven with pyramidal shape. There are some cracks on the PbO_2 electrode surface layer. The EDS result shown in Fig. 2c indicates that the electrode was composed of lead and oxygen. When $[Fe(CN)_6]^{3-}$ was added into the deposition solution as a dopant, some change was observed on FeCN–PbO_2 electrode surface. From Fig. 2b, one can see that the surface of FeCN–PbO_2 electrode was uneven. Some of the crystals were of typical pyramidal shape, and others were of no definite shape. However, there were seldom cracks on the FeCN–PbO_2 electrode surface. As shown in Fig. 2d, it can be found that there were lead, oxygen, iron and nitrogen element on the electrode surface. This indicates that the $[Fe(CN)_6]^{3-}$ anion embedded into the PbO_2 matrix, and a modified electrode was fabricated.

3.1.3. Structure of PbO_2 electrodes

The XRD patterns of these PbO_2 electrodes are shown in Fig. 3. The diffraction peaks observed at $2\theta = 25.4°$, 32.0°, 36.2°, 49.1°, 52.2°, 59.0°, 62.5° and 66.9° are assigned to the (1 1 0), (1 0 1), (2 0 0), (2 1 1), (2 2 0), (3 1 0), (3 0 1) and (2 0 2) plane of β-PbO_2. It can be observed that there is a slight difference between the two XRD patterns. All diffraction peaks were strong and sharp, indicating that the obtained PbO_2 electrodes were well crystallized. However, the intensity of the diffraction peak of FeCN–PbO_2 electrode was stronger than that of PbO_2 electrode and the half-peak width of the reflection peak was diametrical. The average grains sizes of PbO_2 crystals of these two electrodes are shown in Table 1, which were estimated from the half-peak width of the strongest diffraction peak using the Debye–Scherrer equation [5]. The average grain size of FeCN–PbO_2 was 25.1 nm, which was larger than that of PbO_2 (20.4 nm). The results suggest that the modification of $[Fe(CN)_6]^{3-}$ can increase the PbO_2 crystal size. This may explain the reason that the average surface loading amount of β-PbO_2 layer on FeCN–PbO_2 electrode was higher than that on PbO_2 electrode.

3.1.4. Accelerated life test

Fig. 4 shows the time course of cell potential in the accelerated life test for PbO_2 and FeCN–PbO_2 electrodes under 3 mol L^{-1} H_2SO_4 solution with a current density of 500 mA cm^{-2}. According to Fig. 4, one can find that the modification of $[Fe(CN)_6]^{3-}$ anion can obviously extend the lifetime of PbO_2 electrodes. The accelerated lifetime of FeCN–PbO_2 electrode is 287.25 h, which is 1.8 times longer than that of PbO_2 electrode (100.5 h). There are two factors affecting the stability of PbO_2 electrodes. One is the reduction of inner stress in the PbO_2 matrix [21,23]. The EDS result confirmed that the $[Fe(CN)_6]^{3-}$ anion embed into the PbO_2 matrix, which could reduce its inner stress. The other is the electrode average loading amount. The average loading amount was 58.8 and 88.8 mg cm^2 for PbO_2 and FeCN–PbO_2 electrode. The deactivation of PbO_2 electrode is dissolution, detachment and passivation of coating [38]. No detachment was observed during the accelerated life test. Thus the electrode deactivation was attributed to dissolution and passivation. From the point of dissolution, a higher loading amount of oxide led to a longer accelerated lifetime. These resulted in the modified PbO_2 electrode showing a better electrochemical stability.

3.1.5. Electrochemical characterization

The electrochemical activity was positively related to real surface area and the number of active sites accessible to the electrolyte [39]. The voltammetric charge quantity (q^*), which is positively related to real surface area and the number of active sites, can reflect the electrochemical activity of an electrode. For the same electrode material, larger q^* indicates higher electrode activity. We employed the method reported in literature [5,39,40] to calculated q^* for estimating the electrode activity. Fig. 5 shows the relationship of q^* against the reciprocal of square root of scan rate for PbO_2 electrode and FeCN–PbO_2 electrode. The q^* was obtained by integration of the cycle voltammetric curves over the whole potential range from 0 to 2 V. The results indicated that the FeCN–PbO_2 electrode showed a higher voltammetric charge quantity q^* than the PbO_2 electrode. This indicated that the FeCN–PbO_2 electrode had a higher active surface area, which would enhance its electrochemical oxidation ability.

Fig. 6 shows the linear sweep voltammograms of PbO_2 electrode and FeCN–PbO_2 electrode in 0.5 mol L^{-1} H_2SO_4 solution at a scan rate of 20 mV s^{-1}. The oxygen evolution overpotential was 1.858 V and 1.917 V for PbO_2 electrode and FeCN–PbO_2 electrode, respectively. This indicated that the oxygen evolution overpotential of FeCN–PbO_2 electrode was 59 mV higher than that of PbO_2 electrode. The high oxygen evolution overpotential is desired since oxygen evolution is a competitive reaction in the process of anodic oxidation of pollutants [41]. The higher overpotential for oxygen

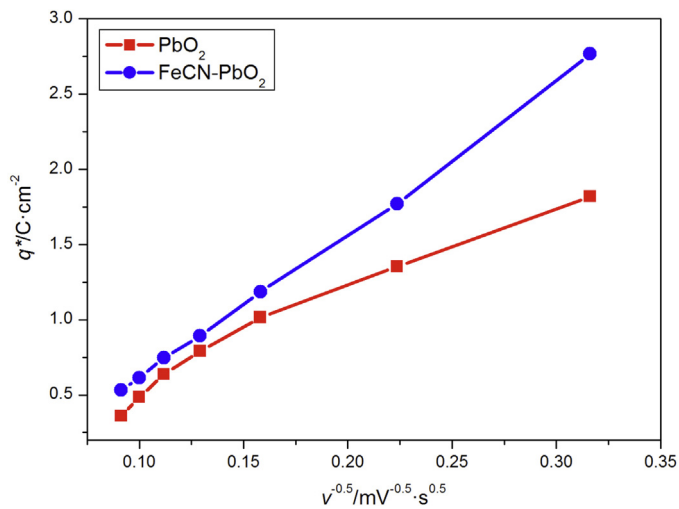

Fig. 5. Relationship of voltammetric charge quantity (q^*) vs. the reciprocal of square root of scan rate in 0.5 mol L^{-1} H_2SO_4 solution.

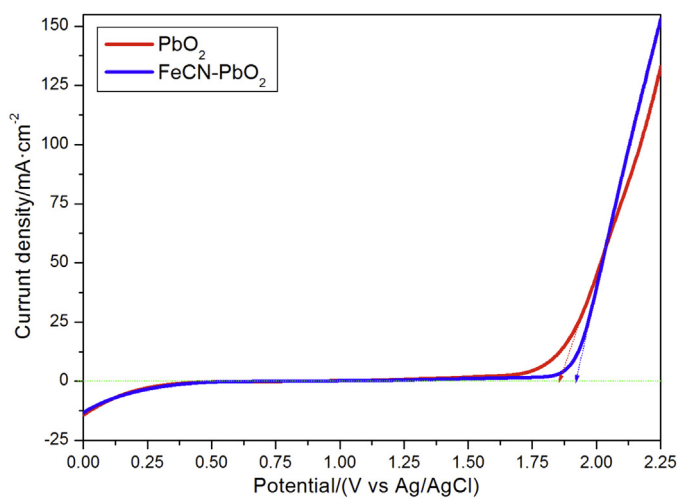

Fig. 6. Linear sweep voltammograms curves of PbO_2 electrode and FeCN–PbO_2 electrode in 0.5 mol L^{-1} H_2SO_4 solution, scan rate: 20 mV s^{-1}.

evolution of FeCN–PbO_2 electrode suggests the higher performance of this electrode than that of PbO_2 electrode on organics degradation.

The effect of $[Fe(CN)_6]^{3-}$ modification on the electrode impedance was analyzed by EIS. The Nyquist plots of freshly prepared PbO_2 and FeCN–PbO_2 are shown in Fig. 7. Qualitatively, the arc diameter for FeCN–PbO_2 is smaller than that for PbO_2, which indicates that the $[Fe(CN)_6]^{3-}$ modification decreased electrode impedance and favors electron transfer. The equivalent circuit which best fits the experimental EIS data is a $R_s(R_fQ)$ combination, as shown in Fig. 7 (the inset image). R_s, R_f, and Q correspond to solution resistance, electrode film resistance and the constant phase element (CPE), respectively [36]. The calculated value of R_s, R_f, and

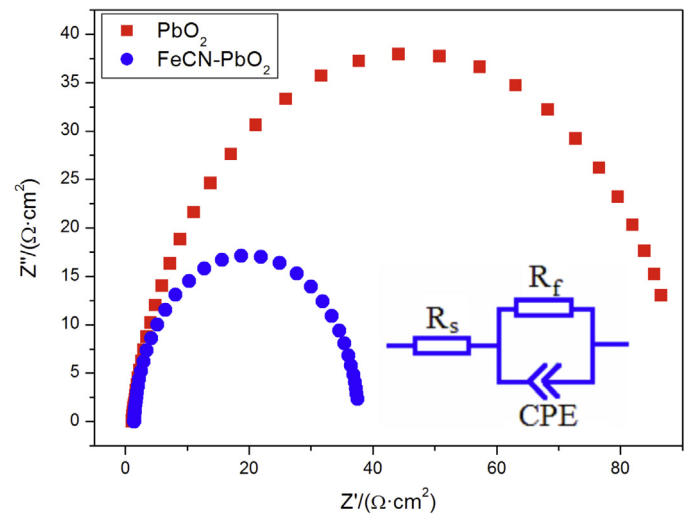

Fig. 7. Nyquist diagrams of PbO_2 and FeCN–PbO_2 electrodes and equivalent circuit used in the analysis of experimental EIS data (the inset image).

Q are shown in Table 1. The R_f value of FeCN–PbO_2 is 36.38 Ω cm^2, which is less than that of PbO_2 (89.8 Ω cm^2). Since the other components are the same, such difference in electrode film resistance could be attributed to the improvement of the surface PbO_2 coating. This indicated that the $[Fe(CN)_6]^{3-}$ modification can reduce the electrode film resistance and reduce the energy consumption.

3.1.6. Electrochemical degradation

To compare the electrochemical degradation activity of the two electrodes, these PbO_2 electrodes were used as the anode in the treatment of aqueous AL solution. The UV_{280} removal efficiency data are shown in Fig. 8a. It can be found in Fig. 8a that the removal efficiency of lignin showed by UV_{280} using FeCN–PbO_2 electrode was 52.25%, which was higher than that of PbO_2 electrode (37.16%). The curves of the normalized absorbance value at 280 nm with degradation time for these two electrodes are shown in the semilogarithmic plots in Fig. 8b. According to the good linear correlation between the logarithm values of the normalized concentration and treatment time, pseudo first-order kinetics can be considered in all cases. As listed in Table 1, the k_{app} value of FeCN–PbO_2 electrode was 0.00609 min^{-1}, which was higher than that of PbO_2 electrode (0.00419 min^{-1}). The FeCN–PbO_2 electrode showed a higher COD removal efficiency and lower energy consumption than that of the PbO_2 electrode. FeCN–PbO_2 electrode exhibited a better degradation performance than the PbO_2 electrode for the degradation of AL as shown in Fig. 8 and Table 1. The higher removal rate for FeCN–PbO_2 electrode can be ascribed to the higher active surface area. FeCN–PbO_2 electrode with larger surface area can provide more active sites centers in the gel layer of the coating to generated more •OH radicals. At the same time, a large surface area of FeCN–PbO_2 electrode increased the adsorption ability of reagent and •OH radicals, which resulted in an improvement on degradation ability of FeCN–PbO_2 electrode [5].

Table 1
Results of different parameters for PbO_2 and FeCN–PbO_2 electrode.

	Crystal size (nm)	R_s (Ω cm^2)	R_f (Ω cm^2)	Q (Ω^{-1} s^n cm^{-2})	n	k_{app} (min^{-1})	R^{2a}	η_{COD} (%)	E_{COD} (kW h $gCOD^{-1}$)
PbO_2	20.4	1.13	89.8	0.0181	0.89	0.00419	0.992	17.8	0.156
FeCN–PbO_2	25.1	1.45	36.4	0.0222	0.96	0.00609	0.993	30.3	0.0885

[a] Correlation coefficient.

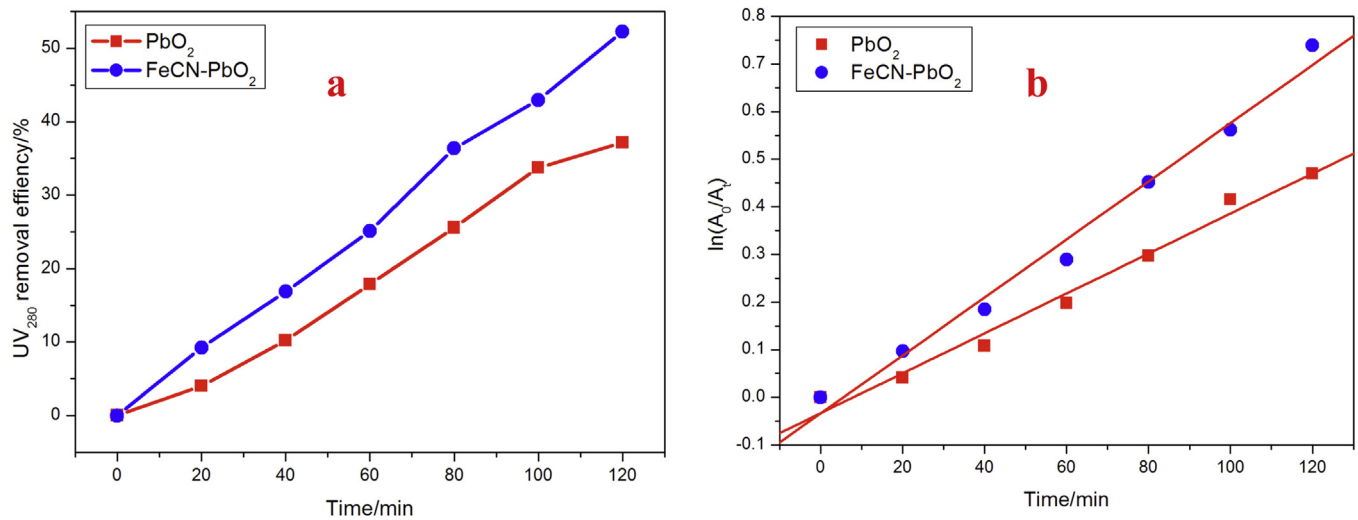

Fig. 8. UV_{280} removal efficiency as a function of degradation time for 200 mg L^{-1} alkali lignin under 20 mA cm^{-2} in 0.5 mol L^{-1} Na_2SO_4 (a) and kinetic coefficient (b).

3.2. Electrochemical oxidation of AL

3.2.1. Applied current density

The degradation of AL on FeCN–PbO_2 electrode may originate from the oxidation by hydroxyl radical formed on the electrode surface. The hydroxyl radical generation capability depends on the applied current density. The effect of applied current density on the electrochemical degradation of AL was investigated. AL concentration was 200 mg L^{-1}, and the degradation process time was 60 min. Fig. S2 presents the plots of UV_{280} removal efficiency and $\ln(A_0/A_t)$ vs. time under different current density. In Fig. S2a, one can see that the UV_{280} removal efficiency significantly increased with the increase of applied current density. The UV_{280} removal efficiency achieved 12.5%, 26.2%, 53.3% and 77.3% at 10, 20, 50 and 100 mA cm^{-2}, respectively, in 60 min electrolysis. A sharp increase in UV_{280} removal efficiency is observed when the current density is lower than 50 mA cm^{-2}. Then a slow increase occurs when the current density was higher than 50 mA cm^{-2}. The semi-log graph of applied current density vs. time is shown in Fig. S2b. The results indicated that the AL degradation at different applied current density ranging from 10 to 100 mA cm^{-2} is in good agreement with the pseudo-first-order model. The parameters of the kinetics are shown in Table 2, and the k_{app} was increased with the increase of current density.

It can be seen in Table 2 that the COD removal efficiency increases with the increase of applied current density. The COD removal efficiency was 7.63%, 12.4%, 19.5% and 21.2% at 10, 20, 50 and 100 mA cm^{-2}, respectively. It is worth pointing out that the COD removal efficiencies were all lower than UV_{280} removal efficiency on different applied current density, indicating that the mineralization of AL was incomplete, and some intermediates were produced.

With the increase of current density, the formation rate of hydroxyl radical increases, which resulted in the increase of the UV_{280} removal efficiency and COD removal efficiency. However, the competitive electrode reaction such as the oxygen evolution is obvious at higher current density. As a result, the EC_{COD} increases from 0.131 kW h $gCOD^{-1}$ of 10 mA cm^{-2} to 0.749 kW h $gCOD^{-1}$ of 100 mA cm^{-2}.

3.2.2. Initial AL concentration

The effect of initial AL concentration on the UV_{280} removal efficiency and $\ln(A_0/A_t)$ vs. time under different initial concentration is shown in Fig. S3. It can be observed in Fig. S3a that the UV_{280} removal efficiency decreased with the increase of initial AL concentration. After 120 min electrolysis, the UV_{280} removal efficiency was 72.1%, 64.7%, 52.3% and 16.7% at initial concentration of 50, 100, 200, 300 mg L^{-1}, respectively. Fig. S3b indicated that

Table 2
Parameters during electrochemical degradation of alkali lignin over FeCN–PbO_2 electrode at different experimental parameters (the applied current density: 20 mA cm^{-2}, the initial alkali lignin concentration: 200 mg L^{-1}, the initial pH 7, the solution temperature: 20 °C).

Applied current density (mA cm^{-2})[a]	10	20	50	100
UV_{280} removal efficiency (%)	12.5	26.2	53.3	77.3
$k_{app} \times 10^3$ (min^{-1})	2.5	5.1	12.9	26.5
R^2[c]	0.987	0.998	0.997	0.995
COD removal efficiency (%)	7.63	12.4	19.5	21.2
EC_{COD} (kW h $gCOD^{-1}$)	0.131	0.184	0.332	0.749

Initial alkali lignin concentration (mg L^{-1})[b]	50	100	200	300
UV_{280} removal efficiency (%)	72.1	64.7	52.3	16.7
$k_{app} \times 10^3$ (min^{-1})	11.5	8.19	6.09	1.39
R^2[c]	0.989	0.986	0.993	0.943
COD removal efficiency (%)	39.7	32.1	30.3	23.2
EC_{COD} (kW h $gCOD^{-1}$)	0.180	0.143	0.0885	0.0769

Initial pH value[b]	3	7	10
UV_{280} removal efficiency (%)	83.7	52.3	43.5
$k_{app} \times 10^3$ (min^{-1})	14.3	6.09	4.65
R^2[c]	0.991	0.993	0.993
COD removal efficiency (%)	40.5	30.3	24.3
EC_{COD} (kW h $gCOD^{-1}$)	0.0638	0.0885	0.111

Solution temperature (°C)[b]	5	10	20	40
UV_{280} removal efficiency (%)	40.4	47.1	52.3	44.6
$k_{app} \times 10^3$ (min^{-1})	4.52	5.38	6.09	5.03
R^2[c]	0.978	0.998	0.993	0.998
COD removal efficiency (%)	16.0	30.0	30.3	39.6
EC_{COD} (kW h $gCOD^{-1}$)	0.239	0.119	0.0885	0.0618

The electrochemical degradation process time: a–60 min; b–120 min.
[c] Correlation coefficient.

the AL degradation at different initial concentrations ranging from 50 to 300 mg L^{-1} is in good agreement with the pseudo-first-order model. The parameters of the kinetics are shown in Table 2. The rate constant (k_{app}) decreased with the increase of AL concentration.

As shown in Table 2, the COD removal efficiency decreases with the increase of initial AL concentration. Although the COD removal efficiency decreases, actual COD removal amount increases with the increase of initial AL concentration. It is also observed that the EC_{COD} for higher initial AL concentration are lower compared with those for lower initial AL concentration. This may be due to the side reaction of oxygen evolution; the radicals could react rapidly with the organic matters before the oxygen evolution in the solution at high initial organic concentration. Because there was no need to mineralize AL into CO_2 in view of cost-effectiveness, electrochemical degradation on FeCN–PbO_2 electrode should be preferable to serve as a pretreated method of the target toxic pollutant for subsequent treatment.

3.2.3. Initial pH

The effect of initial pH values on AL degradation is presented in Fig. S4 and Table 2. The results show that UV_{280} removal efficiency, k_{app} and COD removal efficiency decrease with the increase of initial pH value. The UV_{280} removal efficiency was 83.7%, 52.3% and 43.5% after 120 min, respectively. The COD removal efficiency was 40.5%, 30.3% and 24.3% after 120 min, respectively. From the results, it can be concluded that low pH is beneficial to the degradation of AL.

3.2.4. Solution temperature

The effect of solution temperature on the electrochemical oxidation of AL is presented in Table 2. The UV_{280} removal efficiency increased with temperature from 40.4% at 5 °C to 52.3% at 20 °C. When the temperature increased to 40 °C, the UV_{280} removal efficiency decreased to 44.6%. This may be due to the higher water evaporation rate at higher solution temperature. The COD removal efficiency increased with the increase of temperature from 16.0% at 5 °C to 39.6% at 40 °C, and the EC_{COD} decreased with the increase of temperature from 0.239 kW h $gCOD^{-1}$ at 5 °C to 0.0618 kW h $gCOD^{-1}$ at 40 °C. These results indicated that higher temperatures could enhance the oxidation of organic matters.

4. Conclusion

PbO_2 electrode modified by $[Fe(CN)_6]^{3-}$ anion (marked as FeCN–PbO_2) was prepared by electro-deposition method and used for the electrochemical degradation of alkali lignin (AL). $[Fe(CN)_6]^{3-}$ anion increased the average grain size of lead dioxide and formed a compact surface coating. The service lifetime of FeCN–PbO_2 electrode was 287.25 h, which was longer than that of the unmodified electrode. The electrochemical characterization shows that FeCN–PbO_2 electrode has higher active surface area and oxygen evolution potential than the unmodified electrode, which would benefit its electrochemical oxidation ability. The results of AL electrochemical degradation show that higher applied current density, lower initial AL concentration, lower pH value and higher solution temperature were favorable for the enhancement of UV_{280} removal efficiency and COD removal efficiency of the electrochemical degradation of AL. On the contrary, the results show that a lower EC_{COD} needed lower applied current density, higher initial AL concentration, lower pH value and lower solution temperature.

Acknowledgments

The authors gratefully acknowledge the financial support from the National Natural Science Foundation of China (Grant No. 21307098), China Postdoctoral Science Foundation (Grant No. 2013M532053), and the Fundamental Research Funds for the Central University of PR China.

Appendix A. Supplementary data

Supplementary data associated with this article can be found, in the online version, at http://dx.doi.org/10.1016/j.jhazmat.2014.12.065.

References

[1] C.A. Martinez-Huitle, S. Ferro, Electrochemical oxidation of organic pollutants for the wastewater treatment: direct and indirect processes, Chem. Soc. Rev. 35 (2006) 1324–1340.
[2] C.A. Martínez-Huitle, E. Brillas, Decontamination of wastewaters containing synthetic organic dyes by electrochemical methods: a general review, Appl. Catal. B Environ. 87 (2009) 105–145.
[3] M. Panizza, G. Cerisola, Direct and mediated anodic oxidation of organic pollutants, Chem. Rev. 109 (2009) 6541–6569.
[4] W. Wu, Z.-H. Huang, T.-T. Lim, Recent development of mixed metal oxide anodes for electrochemical oxidation of organic pollutants in water, Appl. Catal. A Gen. 480 (2014) 58–78.
[5] X. Hao, S. Dan, Z. Qian, Y. Honghui, Y. Wei, Preparation and characterization of PbO_2 electrodes from electro-deposition solutions with different copper concentration, RSC Adv. 4 (2014) 25011.
[6] B. Correa-Lozano, C. Comninellis, A.D. Battisti, Electrochemical properties of Ti–SnO_2–Sb_2O_5 electrodes prepared by the spray pyrolysis technique, J. Appl. Electrochem. 26 (1996) 683–688.
[7] X. Li, D. Pletcher, F.C. Walsh, Electrodeposited lead dioxide coatings, Chem. Soc. Rev. 40 (2011) 3879–3894.
[8] S. Chai, G. Zhao, Y. Wang, Y.-n. Zhang, Y. Wang, Y. Jin, X. Huang, Fabrication and enhanced electrocatalytic activity of 3D highly ordered macroporous PbO_2 electrode for recalcitrant pollutant incineration, Appl. Catal. B Environ. 147 (2014) 275–286.
[9] M. Cerro-Lopez, Y. Meas-Vong, M.A. Méndez-Rojas, C.A. Martínez-Huitle, M.A. Quiroz, Formation and growth of PbO_2 inside TiO_2 nanotubes for environmental applications, Appl. Catal. B Environ. 144 (2014) 174–181.
[10] D. Shao, J. Liang, X. Cui, H. Xu, W. Yan, Electrochemical oxidation of lignin by two typical electrodes: Ti/$SbSnO_2$ and Ti/PbO_2, Chem. Eng. J. 244 (2014) 288–295.
[11] K. Pan, M. Tian, Z.H. Jiang, B. Kjartanson, A.C. Chen, Electrochemical oxidation of lignin at lead dioxide nanoparticles photoelectrodeposited on TiO_2 nanotube arrays, Electrochim. Acta 60 (2012) 147–153.
[12] W. Han, C. Zhong, L. Liang, Y. Sun, Y. Guan, L. Wang, X. Sun, J. Li, Electrochemical degradation of triazole fungicides in aqueous solution using TiO_2-NTs/SnO_2–Sb/PbO_2 anode: experimental and DFT studies, Electrochim. Acta 130 (2014) 179–186.
[13] H. Lin, J. Niu, J. Xu, Y. Li, Y. Pan, Electrochemical mineralization of sulfamethoxazole by Ti/SnO_2–Sb/Ce–PbO_2 anode: kinetics, reaction pathways, and energy cost evolution, Electrochim. Acta 97 (2013) 167–174.
[14] Y. Jiang, Z. Hu, M. Zhou, L. Zhou, B. Xi, Efficient degradation of *p*-nitrophenol by electro-oxidation on Fe doped Ti/TiO_2 nanotube/PbO_2 anode, Sep. Purif. Technol. 128 (2014) 67–71.
[15] W. Yang, W. Yang, X. Lin, Research on PEG modified Bi-doping lead dioxide electrode and mechanism, Appl. Surface Sci. 258 (2012) 5716–5722.
[16] O. Shmychkova, T. Luk'yanenko, A. Velichenko, L. Meda, R. Amadelli, Bi-doped PbO_2 anodes: electrodeposition and physico-chemical properties, Electrochim. Acta 111 (2013) 332–338.
[17] H. Xu, J.J. Li, W. Yan, W. Chu, Preparation and characterization of titanium based PbO_2 electrodes doped with some common elements, Rare Metal Mater. Eng. 42 (2013) 885–890.
[18] Y.A. Liu, H.L. Liu, J. Ma, J.J. Li, Investigation on electrochemical properties of cerium doped lead dioxide anode and application for elimination of nitrophenol, Electrochim. Acta 56 (2011) 1352–1360.
[19] J.F. Niu, H. Lin, J.L. Xu, H. Wu, Y.Y. Li, Electrochemical mineralization of perfluorocarboxylic acids (PFCAs) by Ce-doped modified porous nanocrystalline PbO_2 film electrode, Environ. Sci. Technol. 46 (2012) 10191–10198.
[20] Q. Dai, H. Shen, Y. Xia, F. Chen, J. Wang, J. Chen, The application of a novel Ti/SnO_2–Sb_2O_3/PTFE-La-Ce-β-PbO_2 anode on the degradation of cationic gold yellow X-GL in sono-electrochemical oxidation system, Sep. Purif. Technol. 104 (2013) 9–16.
[21] Q. Li, Q. Zhang, H. Cui, L. Ding, Z. Wei, J. Zhai, Fabrication of cerium-doped lead dioxide anode with improved electrocatalytic activity and its application for removal of rhodamine B, Chem. Eng. J. 228 (2013) 806–814.
[22] A.B. Velichenko, V.A. Knysh, T.V. Luk'yanenko, Y.A. Velichenko, D. Devilliers, Electrodeposition PbO_2–TiO_2 and PbO_2–ZrO_2 and its physicochemical properties, Mater. Chem. Phys. 131 (2012) 686–693.
[23] Y. Yao, C. Zhao, J. Zhu, Preparation and characterization of PbO_2–ZrO_2 nanocomposite electrodes, Electrochim. Acta 69 (2012) 146–151.

[24] Y. Yao, C. Zhao, M. Zhao, X. Wang, Electrocatalytic degradation of methylene blue on PbO_2–ZrO_2 nanocomposite electrodes prepared by pulse electrodeposition, J. Hazard. Mater. 263 (2013) 726–734.
[25] Y.W. Yao, T. Zhou, C.M. Zhao, Q.M. Jing, Y. Wang, Influence of ZrO_2 particles on fluorine-doped lead dioxide electrodeposition process from nitrate bath, Electrochim. Acta 99 (2013) 225–229.
[26] Y. Yao, M. Zhao, C. Zhao, H. Zhang, Preparation and properties of PbO_2–ZrO_2 nanocomposite electrodes by pulse electrodeposition, Electrochim. Acta 117 (2014) 453–459.
[27] F.W. Wang, S.D. Li, M. Xu, Y.Y. Wang, W.Y. Fang, X.Y. Yan, Effect of electrochemical modification method on structures and properties of praseodymium doped lead dioxide anodes, J. Electrochem. Soc. 160 (2013) D53–D59.
[28] J.T. Kong, S.Y. Shi, L.C. Kong, X.P. Zhu, J.R. Ni, Preparation and characterization of PbO_2 electrodes doped with different rare earth oxides, Electrochim. Acta 53 (2007) 2048–2054.
[29] A.B. Velichenko, D. Devilliers, Electrodeposition of fluorine-doped lead dioxide, J. Fluorine Chem. 128 (2007) 269–276.
[30] H.Y. Zhao, J.L. Cao, J.Q. Zhang, Effect of fluorine ion doping on performance and electrocatalytic activity of PbO_2 anodes, Chin. J. Inorg. Chem. 23 (2007) 2079–2084.
[31] J. Cao, H. Zhao, F. Cao, J. Zhang, C. Cao, Electrocatalytic degradation of 4-chlorophenol on F-doped PbO_2 anodes, Electrochim. Acta 54 (2009) 2595–2602.
[32] Y. Wang, Z. Shen, Y. Li, J. Niu, Electrochemical properties of the erbium-chitosan-fluorine-modified PbO_2 electrode for the degradation of 2,4-dichlorophenol in aqueous solution, Chemosphere 79 (2010) 987–996.
[33] X. Hong, R. Zhang, S. Tong, C.a. Ma, Preparation of Ti/PTFE-F-PbO_2 electrode with a long life from the sulfamic acid bath and its application in organic degradation, Chin. J. Chem. Eng. 19 (2011) 1033–1038.
[34] R. Tolba, M. Tian, J. Wen, Z.-H. Jiang, A. Chen, Electrochemical oxidation of lignin at IrO_2-based oxide electrodes, J. Electroanal. Chem. 649 (2010) 9–15.
[35] M. Tian, J. Wen, D. MacDonald, R.M. Asmussen, A. Chen, A novel approach for lignin modification and degradation, Electrochem. Commun. 12 (2010) 527–530.
[36] D. Shao, W. Yan, X. Li, H. Yang, H. Xu, A highly stable Ti/TiHx/Sb–SnO_2 anode: preparation, characterization and application, Ind. Eng. Chem. Res. 53 (2014) 3898–3907.
[37] A. Dominguez-Ramos, R. Aldaco, A. Irabien, Electrochemical oxidation of lignosulfonate total organic carbon oxidation kinetics, Ind. Eng. Chem. Res. 47 (2008) 9848–9853.
[38] X. Duan, F. Ma, Z. Yuan, L. Chang, X. Jin, Lauryl benzene sulfonic acid sodium–carbon nanotube-modified PbO_2 electrode for the degradation of 4-chlorophenol, Electrochim. Acta 76 (2012) 333–343.
[39] H.S. Kong, W.M. Huang, H.B. Lin, H.Y. Lu, W.L. Zhang, Effect of SnO_2–Sb_2O_5 interlayer on electrochemical performances of a Ti-substrate lead dioxide electrode, Chin. J. Chem. 30 (2012) 2059–2065.
[40] H.S. Kong, H.Y. Lu, W.L. Zhang, H.B. Lin, W.M. Huang, Performance characterization of Ti substrate lead dioxide electrode with different solid solution interlayers, J. Mater. Sci. 47 (2012) 6709–6715.
[41] D. Shao, X. Li, H. Xu, W. Yan, An improved stable Ti/Sb–SnO_2 electrode with high performance in electrochemical oxidation processes, RSC Adv. 4 (2014) 21230.